Optimal Distribution System Operation for Enhancing Resilience Against Wildfires

Dimitris N. Trakas, *Student Member, IEEE*, and Nikos D. Hatziargyriou, *Fellow, IEEE*

***Abstract*—Natural disasters can cause significant damage to power grids. During summer, in countries with high temperatures, distribution systems passing through forested areas are prone to wildfires. This paper proposes a stochastic programming approach for increasing resiliency of a distribution system exposed to an approaching wildfire. Dynamic line rating of the overhead lines is considered in order to model the impact of the wildfire on conductor temperature and flowing current. The uncertainties associated with solar radiation, wind speed, and wind direction that affect the progression of the wildfire and the production of stochastic distributed generators are taken into account. A scenario reduction algorithm is applied to reduce the number of scenarios in a tractable size and subsequently the computational burden. The proposed model is transformed to a mixed-integer problem with quadratic constraints, which provides effective solution to the operation of a distribution system against an approaching wildfire. A modified IEEE 33-bus distribution system is used to illustrate the applicability of the proposed approach.**

***Index Terms*—Distribution system resilience, dynamic thermal rating, stochastic programming, wildfire.**

NOMENCLATURE

A. Indices and sets

i, j	Indices for buses (1 to N_B).
ij	Distribution line between buses i and j.
t	Index for time periods (1 to N_T).
ω	Index for scenarios (1 to N_Ω).
y	Index of linearization model of $\cos(\vartheta_i - \vartheta_j)$.
$\bar{}$ and $\_$	Symbols for upper and lower bounds.

B. Parameters

1) Flame

L^f	Flame length [m].
γ^f	Flame tilt angle [rad].
T^f	Flame zone temperature [K].
ε^f	Flame zone emissivity.
ρ^b	Fuel bulk density [kg/m^3].

2) Weather and Atmospheric Conditions

V^w	Wind speed [m/s].
φ^w	Angle between the wind direction and the conductor axis [rad].
Φ^s	Solar radiation [W/m^2].
T^a	Ambient temperature [K].
τ	Dimensionless atmospheric transmissivity.
k^a	Thermal conductivity of air [W/mK].
ρ^a	Density of air [kg/m^3].
μ^a	Absolute (dynamic) viscosity of air [kg/ms].

3) Conductor-Line

mC^p	Total heat capacity of conductor [J/mK].
K	Solar absorptivity.
D	Conductor diameter [m].
ε	Conductor emissivity.
L^l	Vertical position of the line [m].
g, b	Conductance and susceptance of line [p.u.].
$T^{\max}$	Conductor maximum permissible temperature [K].

4) Prices, Costs and Values

c^{UP}	Price for buying/selling energy from/to the upstream system [$/MWh].
c^D	Price for selling energy to consumers [$/MWh].
c^G	Generation cost of controllable generators [$/MW].
c^{SU}/c^{SD}	Start-up/Shut-down cost of controllable generators [$].
$VoLL$	Value of lost load [$/MWh].

5) Energy Storage System

n^{ST}	Conversion efficiency of energy storage systems.
EST	Energy capacity of energy storage systems [MWh].

6) Coefficients, Constants and Bounds

λ, β	Coefficients used in the linearization of radiated heat loss rate.
κ, ξ	Coefficients used in the piecewise linearization of $\cos(\vartheta_i - \vartheta_j)$.
B	Stefan-Boltzmann constant [W/(m^{2}K^4)].
$\Delta\vartheta^y_{\min\,/\,\max}$	Lower/Upper bounds of segments for piecewise linearization of $\cos(\vartheta_i - \vartheta_j)$.

7) Others

π	Probability of scenario.
Δt	Duration of time intervals [s].
$M_{1,2,3}$	Sufficiently big positive numbers.

Manuscript received March 7, 2017; revised June 16, 2017; accepted July 22, 2017. Date of publication July 28, 2017; date of current version February 16, 2018. Paper no. TPWRS-00332-2017. *(Corresponding author: Dimitris N. Trakas.)*

The authors are with the Department of Electrical and Computer Engineering, National Technical University of Athens, Athens 10563, Greece (e-mail: dtrakas@power.ece.ntua.gr; nh@power.ece.ntua.gr).

Color versions of one or more of the figures in this paper are available online at http://ieeexplore.ieee.org.

Digital Object Identifier 10.1109/TPWRS.2017.2733224

C. Variables

1) Flame

V^f Fire rate of spread [m/s].
r^f Distance of fire from the line [m].
Φ^f Radiative heat flux emitted from fire [W/m^2].
δ^f View angle between the flame and the conductor [rad].

2) Conductor-Line

T Conductor temperature [K].
$pf^{P/Q}$ Line active/reactive power flow [p.u.].

3) Heat Gain and Loss Rates

q^l Resistive heat gain rate [W/m].
q^s Heat gain rate from sun [W/m].
q^f Heat gain rate from fire [W/m].
q^c Convection heat loss rate [W/m].
q^r Radiated heat loss rate [W/m].

4) Upstream System, Distributed Generation, Energy Storage Systems and Loads

p^{UP} Active power to exchange with the upstream system [p.u.].
$p^{UP_{B/S}}$ Active power to buy/sell from/to the upstream system [p.u.].
$p^{WT/PV/G}$ Active power generation of wind/solar /controllable generators [p.u.].
$p^{ST+/-}$ Charging/Discharging active power for energy storage systems [p.u.].
P^D_ω, Q^D_ω Scenario ω active and reactive power for demand [p.u.].
p^D/q^D Served active/reactive power [p.u.].
$p^{\text{shed}}/q^{\text{shed}}$ Active/Reactive power shedding [p.u.].
q^G Reactive output of controllable generators [p.u.].
q^{ST} Reactive output of energy storage systems [p.u.].
su^G, sd^G Controllable generator start-up and shut-down cost [$].
soc^{ST} State of charge of energy storage systems.

5) Binary Variables

u^l Binary variable for determine the status of line.
u^ζ_{ij} Binary variable for linear approximation of $\cos(\vartheta_i - \vartheta_j)$.
u^{UP} Binary variable for determine of buying or selling energy from/to upstream system.
u^{ST} Binary variable for determine the charging or discharging status of energy storage systems.
u^G Binary variable for determine the status of controllable units.

6) Bus

v Bus voltage magnitude [p.u.].
ϑ Bus voltage angle [rad].

7) Others

K^{angle} Wind direction factor.
N^{Re} Dimensionless Reynolds number.
ζ_{ij} Piecewise linear approximation of $\cos(\vartheta_i - \vartheta_j)$.

For the calculations, the base values of power and voltage are used.

I. Introduction

IN THE light of natural hazards, the necessity for enhancing power grid resilience is gaining increasing attention. Resilience is the grid's ability to withstand extraordinary and high-impact low-probability events that may have never been experienced before, rapidly recover from such disruptive events, and adapt its operation and structure to prevent or mitigate the impact of similar events in the future [1]. The above definition of resilience indicates that a resilient grid must be characterized by fault-tolerance, fast response, recovery and reliability [2]. Natural hazards encompass geological and meteorological phenomena, such as extreme weather events, earthquakes, floods and wildfires. The impacts and financial costs of such events on power grids have led in developing strategies to effectively deal with them [3].

Enhancing power grid resilience can be achieved through hardening and operational measures [4]. Hardening measures have been proposed in [5]–[7]. In [5] a coordinated hardening and distributed generation resource allocation approach is proposed to increase the resilience of the distribution system against a hurricane. In [6] different hardening measures, such as upgrading poles and vegetation management are integrated in a tri-level optimization problem for the minimization of the hardening investment and the projected load shedding cost under extreme weather conditions. A transmission expansion planning for enhancing power system resilience to earthquakes is proposed in [7]. References [8]–[11] propose operational measures for enhancing power grid resilience. An optimal microgrid scheduling considering the probability of an unintentional islanding has been proposed in [8] and [9]. The importance of microgrids in power system resilience enhancement has been highlighted in [2]. In [10] the distribution system is sectionalized into self-supplied microgrids to provide power to the maximum loads of the isolated part in case of faults. An islanded scheme is proposed in [11] to increase power grid resilience against cascading events that are triggered by line damages due to extreme weather.

In the existing literature, the measures for enhancing power grid resilience mainly focus on extreme weather events [5], [6], [11]–[14], while the grids' ability to withstand a wildfire has not been adequately investigated. In [15] a methodology to quantify the damage caused by a wildfire to the distribution system of a city is proposed. However, no measures are proposed for addressing the threat of the fire. The impact of a progressing wildfire on line ratings of a transmission system is proposed in [16]. Moreover, an optimal power flow method for minimizing the generation cost is applied considering reduced line capacities due to the wildfire. In [17], [18] a method for an optimal distribution system operation against a progressing wildfire is presented and the contribution of microgrids and demand response is studied. In [16]–[18] the steady-state heat balance equation is used, that according to IEEE Std 738 [19] it is applied when the electrical current, conductor temperature and weather conditions are assumed constant for all times.

In this paper, optimal distribution system operation for enhancing resilience is formulated and solved considering the varying conditions during the spread of a progressing wildfire and its impact on the system. As stated in [20] and [21], system defense plans and restoration schemes are put in action during emergency situations, to avoid power interruptions and to restore electricity, when interruptions are not avoided. Close coordination between all actors playing an active role in the defense and restoration schemes is required. Distribution System Operators (DSOs) are responsible to supervise and control the implementation of emergency actions. Therefore, it is assumed that during the progression of the wildfire the DSO has full control of distributed generators (DGs) and energy storage systems (ESSs). In fact, according to the German Guideline for generating plants [22], in case of potential danger to system operation security, DSOs are entitled to request a temporary limit of the DGs power or disconnect the facility. Furthermore, DSOs in Great Britain have to prepare and maintain plans for mitigating the effects of an emergency, such as a natural disaster (e.g., wildfire), that may likely disrupt electricity supply [23]. In this case, the Distribution Operating Code sets out Contingency Planning procedures to enable coordination between all the users of the distribution system. In addition, in case of campus or military base, the assumption that the operator is the owner of system components and responsible for their operation is fully applicable [8].

A stochastic programming approach is used to determine the operation of a resilient distribution system exposed in an approaching wildfire. A wildfire is able to cause a direct damage to distribution system components or to decrease thermal rating of the lines due to the increase of the conductor's surface temperature [16]. Dynamic Line Rating (DLR) of the overhead lines is considered in order to model the impact of the wildfire on the conductor's temperature. The non-steady-state heat balance is used to calculate conductor temperature for weather conditions that vary over the time horizon. When the wildfire is within a close distance from the conductors, it is assumed that it disrupts their operation for the rest of the time horizon of the study due to the high rise of their temperature and the violation of their maximum permissible temperature. This does not necessarily mean physical damage, but it can also include unacceptable line sags that leads to the outage of the line.

The main contributions of this paper are:

1) the DLR of overhead lines is integrated in distribution system operation, in order to enhance resilience against an approaching wildfire.
2) the impact of the wildfire on the line's functionality is considered, not only on conductor's temperature, as done in previous publications. This provides a better appraisal of the wildfire effects.
3) the non-steady-state heat balance equation is used to take into account the influence of the wildfire on the conductor's temperature.

The last two terms are original contributions of the proposed method.

The rest of this paper is organized as follows: Section II presents the associated uncertainties. The wildfire model is introduced in Section III. Section IV describes the calculation of the conductor's temperature using the non-steady-state heat balance equation. The proposed approach is presented in Section V and is illustrated in Section VI. Section VII summarizes and concludes the paper.

II. Uncertainties

Distribution systems consisting of ESSs and DGs are considered in this paper. The production of wind turbines (WTs) and photovoltaic panels (PVs) are modeled as stochastic, based on probabilistic forecasting techniques [24], while microturbines (MTs) are modeled as controllable sources.

A. Stochastic Parameters

Wind speed and direction are considered uncorrelated. Weibull and von Mises distributions are used for modelling wind speed and direction [17]. Solar radiation is modelled using Beta distribution and Normal distribution is used for load demand [25]. The parameters of Beta distribution and Weibull distribution are calculated by using their mean value and standard deviation of the predicted solar radiation and wind speed according to [26] and [27], respectively.

B. Scenario Generation and Reduction Algorithm

Monte Carlo simulation (MCs) is used to produce a large number of scenarios for the stochastic parameters based on forecasted values and the typical distribution of each parameter. The use of MCs, instead of simple mean values, is able to provide results covering a whole spectrum of most probable scenario values including worst case probable conditions, as will be shown in Section VI-B. The Backward Scenario Reduction algorithm is then used in order to reduce the number of scenarios in a tractable size [28]. The algorithm is applied iteratively. Based on Kantorovich distance, a scenario is removed at each iteration and its probability is assigned to the closest scenario. The algorithm is terminated when the desired number of scenarios is reached.

III. Wildfire Model

The heat from wildfire is transferred through radiation and convection. In this paper, convective transfer is neglected, since it affects the conductors' temperature, only when the fire is directly under the overhead line. It is most likely however, that a line will already be out of order, when the wildfire is within close distance [17], as mentioned in Section I of the paper.

For a large fire, the simplified heat flux model of [29] is used. The radiative heat flux Φ^f emitted from the fire to a conductor is computed according to:

$$\Phi^f_{ij,\omega,t} = \frac{\tau \varepsilon^f B {T^f}^4}{2} \sin\left(\delta^f_{ij,\omega,t}\right) \tag{1}$$

$$\delta^f_{ij,\omega,t} = \tan^{-1}\left(\frac{L^f \cos\left(\gamma^f\right)}{r^f_{ij,\omega,t} - \left(L^f \sin\left(\gamma^f\right)\right)}\right) \tag{2}$$

where, δ^f is the view angle between the flame and the object threatened by the fire for a large fire front. For a better understanding of (1) and (2), the reader is referred to the schematic geometry used in [29].

The wildfire is moving across the forested area with a specific rate of spread V^f that depends on wind speed V^w and the vegetation of the crossing area.

$$V^f_{\omega,t} = \frac{k\left(1+V^w_{\omega,t}\right)}{\rho^b} \tag{3}$$

where, k is equal to 0.07 kg/m^3 for a wildland fire [16]. The bulk density ρ^b is equal to 40 kg/m^3 along a forest floor. The distance of the wildfire from the conductors at time t depends on wind direction φ^w and the rate of spread V^f:

$$r^f_{ij,\omega,t} = r^f_{ij,\omega,t-1}\ V^f_{\omega,t}\ \Delta t\ \cos(\varphi^w_{ij,\omega,t}) \tag{4}$$

IV. Dynamic Rating of Overhead Lines

The calculation of overhead lines temperature is based on the method presented in IEEE Std 738 [19]. The heat transferred to the conductor from the wildfire is added to the sources that increase the conductor temperature. The change in conductor temperature during the time interval Δt is calculated using the non-steady-state heat balance equation:

$$\left(T_{ij,\omega,t+1} - T_{ij,\omega,t}\right) = \frac{\Delta t}{mC^p}\begin{pmatrix} q^l_{ij,\omega,t} + q^s_{ij,\omega,t} + q^f_{ij,\omega,t} \\ -q^c_{ij,\omega,t} - q^r_{ij,\omega,t}\end{pmatrix} \tag{5}$$

Note that the three first terms, that cause the temperature rise of the conductor, are the heat gain rates due to ohmic losses q^l, solar radiation q^s and radiative heat flux q^f emitted from the fire. These three terms are given by the following equations, respectively:

$$q^l_{ij,\omega,t} = R\left(T_{ij,\omega,t}\right)\left|I_{ij,\omega,t}\right|^2 \tag{6}$$

$$q^s_{ij,\omega,t} = D_{ij}K_{ij}\Phi^s_{ij,\omega,t} \tag{7}$$

$$q^f_{ij,\omega,t} = D_{ij}\Phi^f_{ij,\omega,t} \tag{8}$$

where, $R(T_{ij})$ is a function that describes the dependency of conductor resistance form its temperature and I_{ij} is the line current.

The last two terms in (5) cool down the conductor. The convection q^c for non-zero wind speeds and radiative heat loss q^r rates are calculated according to:

$$q^c_{ij,\omega,t} = \max\begin{pmatrix} K^{\text{angle}}_{ij,\omega,t}\left[1.01+1.35\left(N^{Re}_{ij,\omega,t}\right)^{0.52}\right]\left(T_{ij,\omega,t}-T^a_{ij,t}\right) \\ K^{\text{angle}}_{ij,\omega,t}0.754\left(N^{Re}_{ij,\omega,t}\right)^{0.6}k^a\left(T_{ij,\omega,t}-T^a_{ij,t}\right)\end{pmatrix} \tag{9}$$

$$q^r_{ij,\omega,t} = 17.8D_{ij}\varepsilon\left[\left(\frac{T_{ij,\omega,t}}{100}\right)^4 - \left(\frac{T^a_{ij,t}}{100}\right)^4\right] \tag{10}$$

The magnitude of the convective heat loss q^c depends on a dimensionless number N^{Re} known as Reynolds number and the wind direction factor K^{angle} that are given by:

$$N^{Re}_{ij,\omega,t} = \frac{D_{ij}\rho^\alpha V^w_{\omega,t}}{\mu^\alpha} \tag{11}$$

$$K^{\text{angle}}_{ij,\omega,t} = 1.194 - \cos\left(\varphi^w_{ij,\omega,t}\right) + 0.194\ \cos\left(2\varphi^w_{ij,\omega,t}\right) + 0.368\ \sin\left(2\varphi^w_{ij,\omega,t}\right) \tag{12}$$

Equation (9) is used for non-zero winds. In the present paper, the burst and progression of a wildfire caused by high wind speeds is modeled, thus zero-wind speed is not considered.

Equations (1)–(4), (11), (12) depend only on problem parameters and are calculated after the application of the generation and scenario reduction algorithm, in order to be used as inputs to the optimization problem. In addition, the generation of WTs and PVs that are used as inputs to the optimization problem are calculated according to [25].

V. Problem Formulation

A. Optimization Problem for Resilient Operation Against Approaching Wildfire

A stochastic programming formulation is used for enhancing distribution system resilience against an approaching wildfire. The optimization problem is expressed as:

$$\begin{aligned}\min &\sum_{t=1}^{N_T}\sum_{\omega=1}^{N_\Omega}\pi_\omega\sum_{i=1}^{N_B}\left(VoLLp^{\text{shed}}_{i,\omega,t} - c^D p^D_{i,\omega,t}\right) \\ &+\sum_{t=1}^{N_T}\sum_{\omega=1}^{N_\Omega}\pi_\omega\sum_{i=1}^{N_B}\left(c^G p^G_{i,\omega,t}\right) \\ &+\sum_{t=1}^{N_T}\sum_{\omega=1}^{N_\Omega}\pi_\omega c^{UP}_t\left(p^{UP_B}_{\omega,t} - p^{UP_S}_{\omega,t}\right) \\ &+\sum_{t=1}^{N_T}\sum_{i=1}^{N_B}\left(su^G_{i,t}+sd^G_{i,t}\right)\end{aligned} \tag{13}$$

$$\begin{aligned}&p^G_{i,\omega,t} + p^{WT}_{i,\omega,t} + p^{PV}_{i,\omega,t} + p^{ST-}_{i,\omega,t} - p^{ST+}_{i,\omega,t} - p^D_{i,\omega,t} \\ &\quad = \sum_{j=1}^{N_B} pf^P_{ij,\omega,t}\end{aligned} \tag{14}$$

$$q^G_{i,\omega,t} + q^{ST}_{i,\omega,t} - q^D_{i,\omega,t} = \sum_{j=1}^{N_B} pf^Q_{ij,\omega,t} \tag{15}$$

$$\underline{p^G_i}u^G_{i,t} \le p^G_{i,\omega,t} \le \overline{p^G_i}u^G_{i,t} \tag{16}$$

$$\underline{q^G_i}u^G_{i,t} \le q^G_{i,\omega,t} \le \overline{q^G_i}u^G_{i,t} \tag{17}$$

$$su^G_{i,t} \ge 0,\ su^G_{i,t} \ge c^{SU}_i\left(u^G_{i,t} - u^G_{i,t-1}\right) \tag{18}$$

$$sd^G_{i,t} \ge 0,\ sd^G_{i,t} \ge c^{SD}_i\left(u^G_{i,t-1} - u^G_{i,t}\right) \tag{19}$$

$$T_{ij,\omega,t} \le T^{\max}_{ij} + \left(1-u^l_{ij,\omega,t}\right)M_1 \tag{20}$$

$$-M_2u^l_{ij,\omega,t} \le pf^P_{ij,\omega,t} \le M_2u^l_{ij,\omega,t} \tag{21}$$

$$-M_2 u^l_{ij,\omega,t} \le pf^Q_{ij,\omega,t} \le M_2 u^l_{ij,\omega,t} \tag{22}$$

$$\begin{aligned} &- M_3\left(1-u^l_{ij,\omega,t}\right) \le \\ &pf^P_{ij,\omega,t} - \left(g_{ij}\left(v_{i,\omega,t}-v_{j,\omega,t}-\zeta_{ij,\omega,t}+1\right)\right. \\ &\qquad \left. - b_{ij}\left(\vartheta_{i,\omega,t}-\vartheta_{j,\omega,t}\right)\right) \\ &\le M_3\left(1-u^l_{ij,\omega,t}\right) \end{aligned} \tag{23}$$

$$\begin{aligned} &- M_3\left(1-u^l_{ij,\omega,t}\right) \le \\ &pf^Q_{ij,\omega,t} - \left(-b_{ij}\left(v_{i,\omega,t}-v_{j,\omega,t}-\zeta_{ij,\omega,t}+1\right)\right. \\ &\qquad \left. - g_{ij}\left(\vartheta_{i,\omega,t}-\vartheta_{j,\omega,t}\right)\right) \\ &\le M_3\left(1-u^l_{ij,\omega,t}\right) \end{aligned} \tag{24}$$

$$\zeta_{ij,\omega,t} = \sum_y \left(\kappa_{ij,\omega,t,y}\Delta\vartheta_{ij,\omega,t,y} + u^{\zeta}_{ij,\omega,t,y}\xi_{ij,\omega,t,y}\right) \tag{25}$$

$$\sum_y u^{\zeta}_{ij,\omega,t,y} = 1 \tag{26}$$

$$\Delta\vartheta^y_{\min} u^{\zeta}_{ij,\omega,t,y} \le \Delta\vartheta_{ij,\omega,t,y} \le u^{\zeta}_{ij,\omega,t,y}\Delta\vartheta^y_{\max} \tag{27}$$

$$\sum_y \Delta\vartheta_{ij,\omega,t,y} = \vartheta_{i,\omega,t} - \vartheta_{j,\omega,t} \tag{28}$$

$$u^l_{ij,\omega,t} \le u^l_{ij,\omega,t-1} \tag{29}$$

$$\underline{v_i} \le v_{i,\omega,t} \le \overline{v_i} \tag{30}$$

$$0 \le p^{\text{shed}}_{i,\omega,t} \le P^D_{i,\omega,t} \tag{31}$$

$$q^{\text{shed}}_{i,\omega,t} = p^{\text{shed}}_{i,\omega,t}\frac{Q^D_{i,\omega,t}}{P^D_{i,\omega,t}} \tag{32}$$

$$soc^{ST}_{i,\omega,t} = soc^{ST}_{i,\omega,t-1} + \frac{n^{ST}_i p^{ST+}_{i,\omega,t}\frac{\Delta t}{3600}}{E^{ST}_i} - \frac{p^{ST-}_{i,\omega,t}\frac{\Delta t}{3600}}{n^{ST}_i E^{ST}_i} \tag{33}$$

$$\underline{SOC^{ST}_i} \le soc^{ST}_{i,\omega,t} \le \overline{SOC^{ST}_i} \tag{34}$$

$$0 \le p^{ST+}_{i,\omega,t} \le \overline{p^{ST+}_i}\, u^{ST}_{i,\omega,t} \tag{35}$$

$$0 \le p^{ST-}_{i,\omega,t} \le n^{ST}_i \overline{p^{ST-}_i}\left(1-u^{ST}_{i,\omega,t}\right) \tag{36}$$

$$\underline{q^{ST}_i} \le q^{ST}_{i,\omega,t} \le \overline{q^{ST}_i} \tag{37}$$

$$soc^{ST}_{i,\omega,t_{\text{end}}} \ge soc_{\text{thres}} \tag{38}$$

$$p^{UP}_{\omega,t} = p^{UP_B}_{\omega,t} - p^{UP_S}_{\omega,t} \tag{39}$$

$$0 \le p^{UP_B}_{\omega,t} \le \overline{P^{UP_B}}\, u^{UP}_{\omega,t} \tag{40}$$

$$0 \le p^{UP_S}_{\omega,t} \le \overline{P^{UP_S}}\left(1-u^{UP}_{\omega,t}\right) \tag{41}$$

$$p^D_{i,\omega,t} = P^D_{i,\omega,t} - p^{\text{shed}}_{i,\omega,t} \tag{42}$$

$$q^D_{i,\omega,t} = Q^D_{i,\omega,t} - q^{\text{shed}}_{i,\omega,t} \tag{43}$$

and (5)–(10).

The objective function (13) aims to minimize the expected social cost, expressed as a minimum load shedding during an emergency situation, such as an approaching wildfire, for the next hours, in the most efficient way and respecting operating limits of the system. Although resilience is directly associated with minimum load shedding [11], [12], the method also considers operating costs in order to provide the most economic solutions. The first term represents the load shedding cost minus the retailers' revenue for selling energy to customers. The second term represents the generation cost of MTs units. The third term describes the cost of power exchange with the upstream system. The fourth term represents start-up and shut-down costs of MTs units. The MTs are controlled according to the proposed scheduling and therefore the MTs' status is the same at each scenario. Thus, the start-up and shut-down costs of MTs are not associated with the scenarios. The value of lost load is set large enough, in order to prioritize the demand satisfaction. It is noted that the revenue from selling energy to customers and the cost of power exchange with the upstream system are attributed to retailers. DSO does not benefit from system operation and cannot make revenues.

Constraints (14) and (15) guarantee the active and reactive power balance at each bus, including the power exchange at the point of common coupling. Constraints (16)–(19) represent the active and reactive output limits of MTs and their start-up and shut-down costs, respectively. Constraint (20) sets the conductor out of order, when its temperature exceeds the maximum permissible temperature $T^{\max}$ (if $u^l = 0$, the conductor is set out of order). In this case, it is assumed that the wildfire is very close, and therefore the conductor is outaged by the fire. Constraints (21)–(28) represent power flow equations. Constraints (21) and (22) allow the power flow through the line only when the line is functional. The selection of M_2 should allow the maximum flow of the line. Equations (23) and (24) are converted to equalities when the line is functional and relate voltage magnitude and angle to power flow. The linearization of power flow equations proposed in [8] is used, where $\zeta_{ij,\omega,t}$ represents the piecewise linear approximation of $\cos(\vartheta_i - \vartheta_j)$. More details about the linearization of power flow equations and their accuracy can be found in [30] and [31]. Constraints (25)–(28) describe the proposed piecewise linearization approximation. The number of pieces is selected as a trade-off between computation time and accuracy of the linearized power flow equations. M_1 and M_3 are activated when the lines are outaged and are suitably selected in order to allow the conductor to reach high temperature due to the fire and the calculation of voltages and angles of the buses at the ends of lines set out of order. Constraint (29) guarantees that if a line is outaged due to the fire, it will remain off-line for the rest of the time horizon. Constraint (30) guarantees that bus voltages are within limits. Constraints (31) and (32) represent the load shedding bounds considering constant power factor loads. Equations (33)–(38) describe the operation and limits of ESSs. The state of charge of ESSs is calculated by (33). Equation (34) guarantees that state of charge of ESSs is within the permissible limits. Equations (35) and (36) represent the active power limits of ESSs depending on their operation mode. Constraint (37) represents the reactive output limits of ESSs. Constraint (38) is used in order to maintain the SOC of ESSs above a prespecified threshold soc_{thres} at the end of the time horizon t_{end}. Constraints (39)–(41) model the power exchange with the

upstream system. Constraint (39) represents the amount of exchanged power with the upstream system. Constraints (40) and (41) describe the power exchange limits depending on the mode of the distribution system (exporting or importing electricity). Constraints (42) and (43) express the actually served load, that is equal to the scenario load demand minus the load shed.

The problem expressed in (13) is highly non-linear and non-convex due to (6), (9) and (10). Section V-B presents the procedure for transforming the problem to a mixed integer problem with quadratic constraints.

B. Convexification of Nonconvex Terms

To convexify the non-convex terms (6), (9) and (10), they are transformed according to [32]. The heat gain rate due to ohmic losses, given in (6), is equal to the product of the square of the current flow and its resistance. The resistance of the conductor is given by:

$$R_{ij,\omega,t}\left(T_{ij,\omega,t}\right) = R_{ij,\mathrm{ref}}\left(1 + d_{ij}\left(T_{ij,\omega,t} - T_{ij,\mathrm{ref}}\right)\right) \quad (44)$$

where, $R_{ij,\mathrm{ref}}$ is the conductor resistance at the reference temperature $T_{ij,\mathrm{ref}}$ and d_{ij} is the conductor thermal resistivity coefficient. Considering that the resistance of the conductor is constant and equal to the one obtained for its maximum permissible temperature $T_{ij}^{\max}$ and the voltage is close to 1 p.u., (6) can be transformed to an inequality given by:

$$q_{ij,\omega,t}^{l} \geq R_{ij,\omega,t}\left(T_{ij}^{\max}\right)\left(\left|pf_{ij,\omega,t}^{P}\right|^2 + \left|pf_{ij,\omega,t}^{Q}\right|^2\right) \quad (45)$$

The heat loss rate, given in (10), is linearized and is given by:

$$q_{ij,\omega,t}^{r} = \lambda\, T_{ij,\omega,t} + \beta \quad (46)$$

The convection heat loss rate in (9) can be expressed as a function of the difference between the conductor temperature and the ambient temperature, multiplied by a slope. The maximum calculated slope in (9) is used as input to the optimization problem.

In this way, the optimization problem is transformed to a mixed integer problem with quadratic constraints and can be solved using a commercial solver.

C. Framework of the Proposed Method

As a first step, MCs is used to produce a large number of scenarios. The typical distributions of stochastic parameters (Section II-A) are used for each scenario. Backward Scenario Reduction Algorithm is then applied to reduce the number of scenarios and subsequently the computation efforts. In the next step, using the generated scenarios, the radiative heat flux emitted from the fire, the generation of stochastic generators and the parameters of convection heat loss rate are computed in order to be used as inputs to the optimization problem. Finally, the optimization problem for resilient operation against approaching wildfire is solved. The overall proposed methodology is illustrated in Fig. 1.

STAGES	TASKS
Scenario Generation and Reduction Algorithm	• Generate a large number of scenarios using MCs • Reduce the number of scenarios using Backward Scenario Reduction Algorithm
Prepare Data for Optimization Problem	• Compute fire heat flux • Compute wind and solar generation • Compute parameters of convection heat loss rate
Optimize Distribution System Operation	• Solve stochastic problem for enhancing distribution system resilience against approaching wildfire

Fig. 1. Framework of the proposed approach.

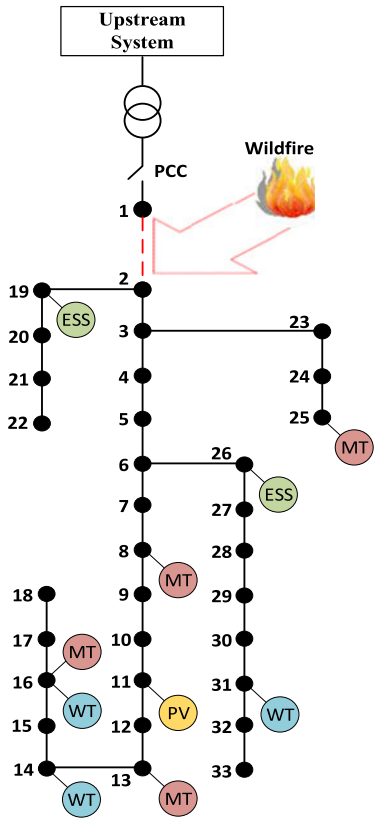

Fig. 2. Single-line diagram of the simulated distribution system and wildfire progression.

VI. Case Study Application

A. Test Network and Simulation Data

This section presents the results of the proposed method applied to a modified IEEE 33-bus distribution system [33]. The system is assumed balanced and is represented by an equivalent single-phase circuit. The single line diagram of the modified network and the progression of the wildfire are presented in Fig. 2. The peak active demand is equal to 15 MW, constant power factor loads are considered and the load profile for the summer season is adopted from [34]. The distribution system extends to a small geographical region, therefore its components are exposed to similar weather conditions. The location and capacity of the system components are shown in Table I. The data of MTs and ESSs are the same used in [8]. The parameters

TABLE I
LOCATION AND CAPACITY OF DISTRIBUTION SYSTEM COMPONENTS

Type	Bus	Capacity (MW)
WTs	14/16/31	0.8/0.8/0.8
PV	11	0.5
MTs	8/13/16/25	3/2/2/3
ESSs	19/26	0.5/0.5

TABLE II
PARAMETERS OF ENERGY STORAGE SYSTEMS

Energy Storage System	E^{ST} (MWh)	$\overline{p^{ST+/-}}$ (MW)	$\overline{q^{ST}}$ (MVAr)	$\underline{q^{ST}}$ (MVAr)
ESS (bus 19)	1.5	0.5	0.3	−0.3
ESS (bus 26)	1.5	0.5	0.3	−0.3

of ESSs are shown in Table II. For WTs, the cut-in, cut-out and rated wind speeds are 4, 20 and 12 m/s, respectively. The rated illumination intensity of the PVs is 1000 W/m^2. The standard deviation is considered equal to 15% of the mean value for wind speed and solar radiation and 5% of the mean value for the loads. A k-factor of 2 is assumed for the von Mises distribution. The weather parameters and wildfire data are taken from [16]. A time step of 30 min is selected, that according to [32] is a tolerable time step for DLR modeling. The wind and the solar data are obtained from [35] and [36], respectively.

A summer day with high wind speed and ambient temperature that facilitate the development and spread of a wildfire is considered. It is assumed that the fire breaks out at $t = 1$, approaches and affects only the line between buses 1 and 2 (red dashed line in Fig. 2). The proposed method can be applied at any time during the day at which the threat of the wildfire is perceived. Therefore, in the light of a wildfire threat, the scheduled operation changes to enhance distribution system resilience. The initial distance from the line is $r^f_{t=1} = 1200$ m. The rest of the lines are considered at a safe distance from the fire. The selected line is the one that connects the distribution system with the upstream network and therefore the power exchange between the two systems is affected by the fire. The proposed method is general however and it can be applied for the study of any line or lines approached by the fire. Assuming that the spatial data of the distribution system are known, e.g., by a Geographic Information System (GIS), the distance between the fire and the conductors can be estimated, during the progression of the wildfire. Based on the estimated distance, the impact of the wildfire on the temperature of any line can be computed.

It is considered that at the end of the time horizon, the wildfire is extinguished, but the affected line remains out of service until it is repaired. Thus, the SOC of the ESSs is required to remain greater than 30% of the maximum capacity, in order to contribute to demand satisfaction for the next hours after the study.

An ASCR type conductor is considered. The diameter and the maximum permissible temperature of the line is assumed equal to 21 mm and 353 K, respectively.

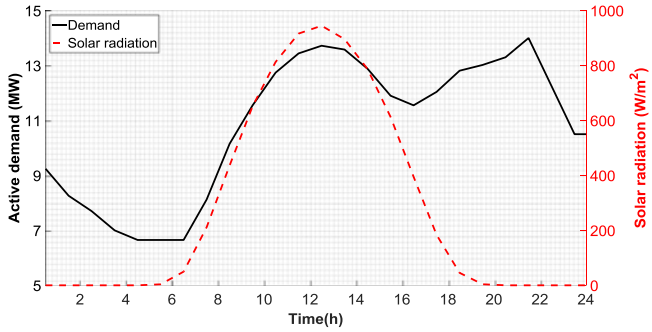

Fig. 3. Mean value of active demand and solar radiation.

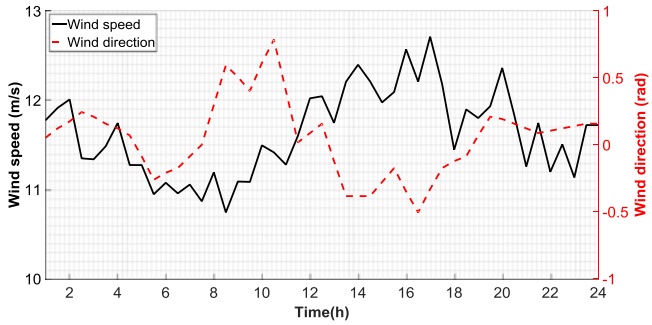

Fig. 4. Mean value of wind speed at L^{WT} and wind direction.

Twenty pieces are used for the piecewise linear approximation of $\cos(\vartheta_i - \vartheta_j)$ in the linearized power flow equations. One thousand scenarios have been generated using Monte Carlo simulation. The appropriate number of representative scenarios has been selected taking into account the range of optimization results (their impact on the objective function) and the required computation time. In our application, 10 representative scenarios are the best choice, since a higher number has an insignificant effect on the results and the computation time becomes unacceptably high for on-line application of the method. The selection of 10 representative scenarios is further discussed in the Appendix.

The mean value of active demand and solar radiation are presented in Fig. 3. Fig. 4 presents the mean values of wind speed and wind direction. The angle is measured with respect to the axis defined by the fire and the conductor. Wind speed $V^{w,WT}$ in Fig. 4 refers to the height L^{WT} of WTs. The wind speed at L^l is given by [37]:

$$V^{w,l} = V^{w,WT}\left(\frac{L^l}{L^{WT}}\right)^{0.143} \tag{47}$$

The ambient temperature and the price of power exchange with the upstream system are presented in Fig. 5. The price of buying and selling energy from and to the upstream system is considered equal and is adopted from [9].

The proposed model was solved using GAMS IDE and IBM CPLEX solver. A PC with Intel Core i7 CPU @3.40 GHz and 4 GB RAM was used. The computation time was 973.074 s.

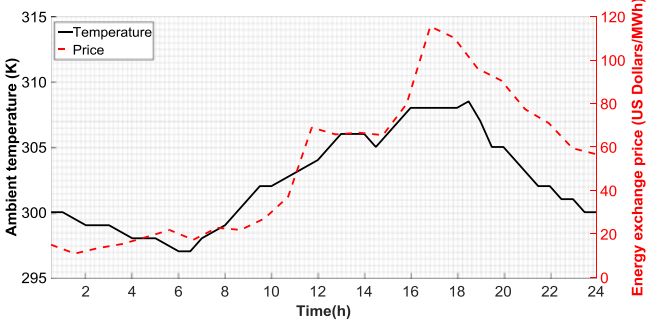

Fig. 5. Ambient temperature and power exchange price.

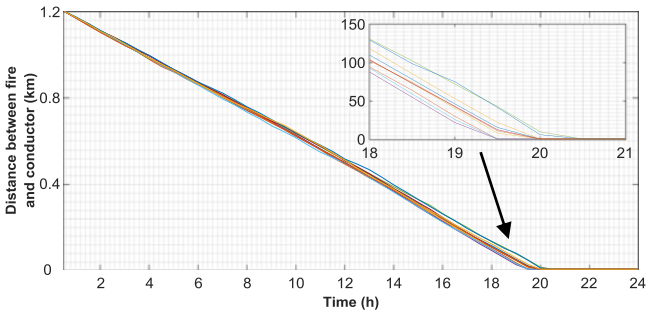

Fig. 6. Distance between fire and line 1-2 in the reduced number of scenarios and magnified subfigure.

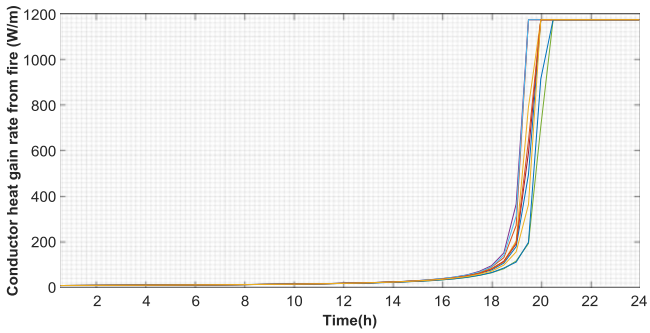

Fig. 7. Conductor 1-2 heat gain rate form fire in the reduced number of scenarios.

B. Operation Against Approaching Wildfire

The proposed method is applied in order to optimize distribution system operation for enhancing its resilience against the approaching wildfire for the next 24 hours. Fig. 6 shows the distance between the fire and line 1-2. It is observed that the fire approaches the line during the day reaching zero distance in the last hours. Fig. 7 presents the conductor heat gain rate from the fire. By comparing Figs. 6 and 7, it is observed that the conductor heat gain rate from the fire gets values greater than zero when the distance of the fire from the line is less than 300 m and increases exponentially, as the fire approaches the line. Figs. 6 and 7 also show the added value of the stochastic analysis. In Fig. 6, for example, it is observed that the wildfire reaches to a close distance from the line, (less than 15 m), in different time steps for each examined scenario. As a result, application of a deterministic optimization based on mean forecasted values, would not consider the line outage at an earlier, yet probable time step.

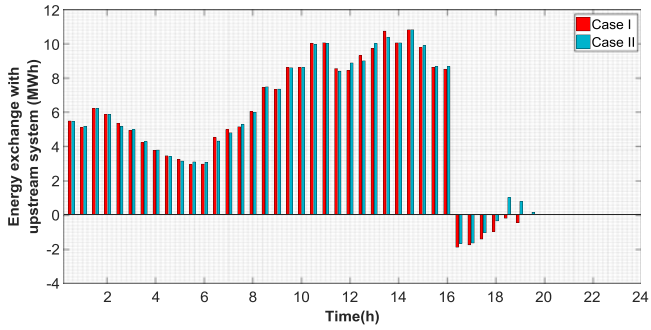

Fig. 8. Expected energy exchange with the upstream system for *Cases I* and *II*.

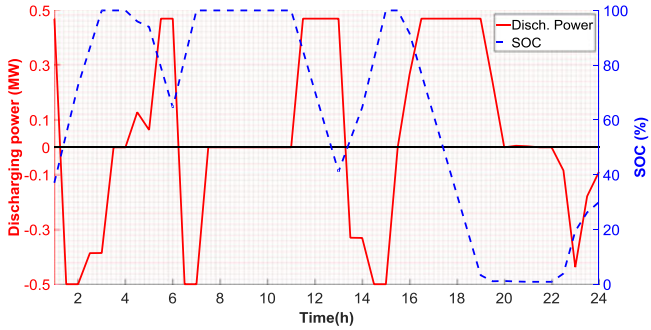

Fig. 9. Expected discharging power and SOC of ESS at bus 19 for *Case I*.

Two cases are considered in order to evaluate the effectiveness of the proposed method. In *Case I* the distribution system operation is optimized to minimize social cost without considering the wildfire progression. In *Case II* the wildfire progression is considered and the resilient operation of the distribution system is optimized.

The expected energy exchange with the upstream system for both cases is presented in Fig. 8. It is observed that until 16:00 hour, the energy exchange is almost identical for both cases and energy is bought from the upstream system since the price of power bought is lower than the cost of the local MTs and the power from renewable generators does not cover the demand. After 16:00 hour and until 18:00, the power exchange price has high values and therefore energy is sold to the upstream system. For *Case I* the exchanged energy is higher because as shown in Fig. 9 the ESS injects active power equal to its higher capacity in order to maximize the revenues from selling energy to the upstream system. For *Case II*, as shown in Fig. 10, the discharging power of ESSs is lower since it is desired to maintain the SOC in the necessary level in order the discharging power of ESSs to be used for minimizing load shedding when the connection with the upstream system will be disrupted due to the wildfire. After 18:00 hour and until 19:30, the power exchange price is lower but still higher than the cost of the local MTs. For *Case I* the operator continues to sell energy to the upstream, while for *Case II* energy is bought for charging the ESSs before line 1-2 is outaged due to the wildfire.

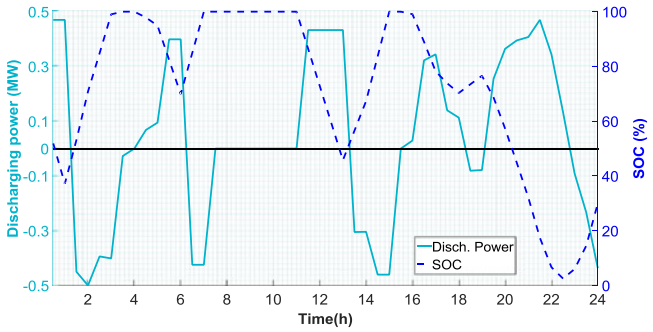

Fig. 10. Expected discharging power and SOC of ESS at bus 19 for *Case II*.

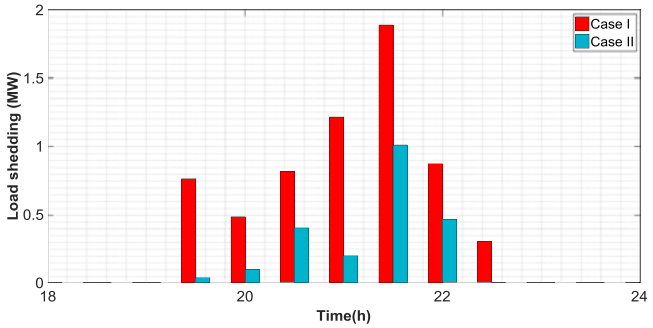

Fig. 11. Expected load shedding for *Cases I* and *II*.

After this time, the power exchange with the upstream system drops to zero, since the line 1-2 is set out of order due to the violation of its maximum temperature. As a result of the strategy that was followed in *Case I*, the SOC of the ESS at bus 19 is at its lowest level. Meanwhile, for *Case II* the ESSs are charged to the desired levels in order to serve the demand during the time the distribution system is disconnected from the upstream system and minimize the load shedding.

Fig. 11. presents the expected amount of load that is shed to keep the balance between generation and demand, when line 1-2 is outaged. Until 19:00 hour, load is not shed in both cases. Between 19:30 and 22:30, an amount of load is shed due to the disconnection of line 1-2 and the inability of the DGs and ESSs to meet the demand. For *Case II* the amount of load shedding is much lower due to the proper operation of the ESSs before the disconnection of line 1-2. After 23:00 hour, the demand is met by the DGs and load shedding is not recorded for both cases. Moreover, the ESSs are charged to reach the required levels.

Fig. 12 shows the voltage at bus 33 for *Case II* (minimum recorded voltage). The minimum voltage is recorded during the disconnection of line 1-2. It is observed that the reactive power injected by the MTs and ESSs is able to keep the voltage within permissible limits during the isolation of the distribution system. After the 22:00 hour, the voltage increases, as the load decreases (see Fig. 3).

Table III presents the load shedding cost, the revenue from selling energy to customers, the cost of power exchange with the upstream system and the generation cost for both cases. Furthermore, *Case III* is considered, where the wildfire progression is taken into account, but only load shedding is minimized without

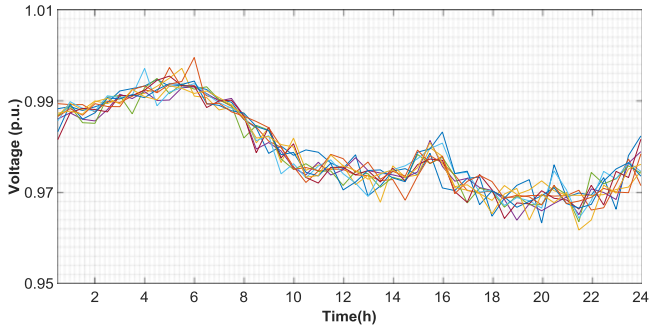

Fig. 12. Bus 33 voltage in the reduced number of scenarios for *Case II*.

TABLE III
REVENUES AND COSTS FOR *Cases I*, *II*, AND *III* ($\$\times 10^3$)

Case	Load shedding cost	Generation cost	Power exchange cost	Revenue from selling energy to customers
I.	3.16	8.24	4.29	77.16
II.	1.23	8.29	4.43	77.75
III.	1.23	17.82	0.71	77.75

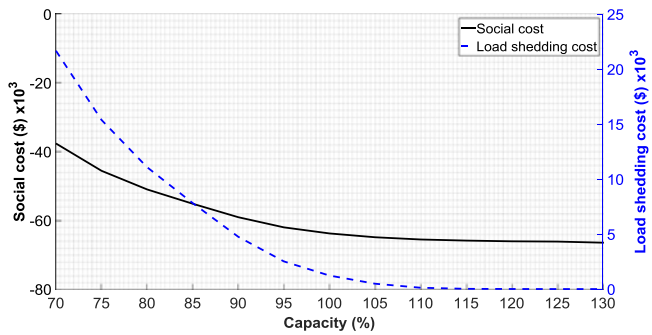

Fig. 13. Objective function value and load shedding cost considering variation of installed power ratings.

consideration of other costs in (13). The value of lost load $VoLL$ is set at 1000 \$/MWh [17], [38], in order to prioritize demand satisfaction. Load shedding cost for *Case II* and *III* is identical, since for both cases the priority is to minimize load shedding, while for *Case I* load shedding cost is higher, as expected. The higher load shedding in *Case I* results in lower revenue from selling energy to customers. For *Case II*, power exchange cost and generation cost are slightly higher than *Case I* due to the energy used to charge the ESSs before disconnection of line 1-2. Generation cost for *Case III* is much higher due to the formulation of the objective function.

C. Effects of Capacity and Location of DGs and ESSs

The rated powers of the system components in Table I are varied from 70% to 130% in steps of 10% compared to *Case II*. The value of the objective function (social cost) and the load shedding cost are presented in Fig. 13. As expected, the value of the objective function and the load shedding cost decrease as the installed capacities increase. When the overall capacity exceeds 110%, load shedding cost reaches zero and the

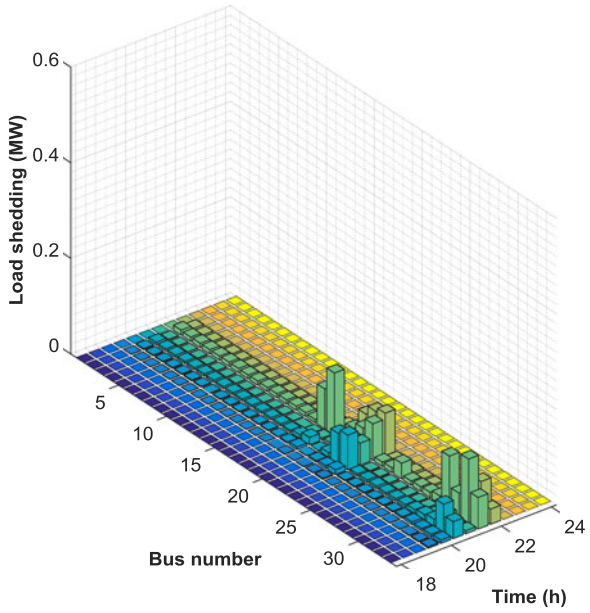

Fig. 14. Spatial expected load shedding for *Case II.*

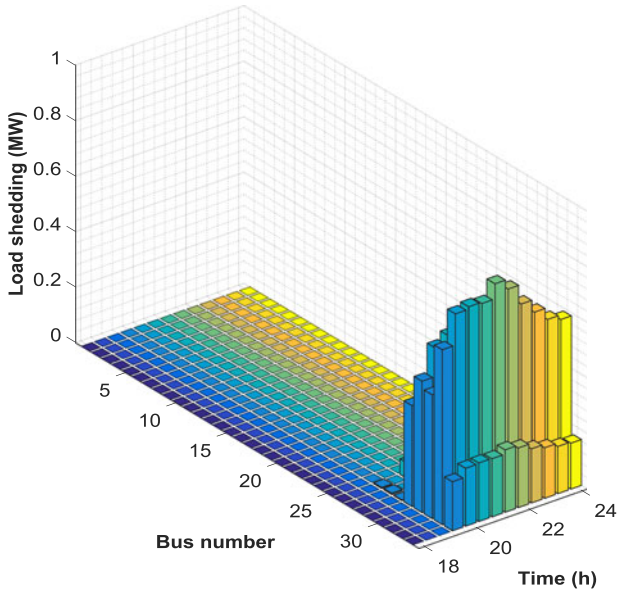

Fig. 15. Spatial expected load shedding for *Case IV.*

value of the objective function decreases at a much lower rate. Further decrease of the social cost is mainly due to the increase of the energy provided to the upstream system before the outage of line 1-2.

The location of the distribution system components, in combination with the affected lines by the wildfire, have a high influence on load shedding. In particular, the presence of DGs and ESSs in an isolated part of the distribution system after the wildfire, is critical for maintaining demand supply and minimize load shedding. For example, in case the wildfire affects line between buses 19 and 20, the demand of buses 20, 21 and 22 will not be satisfied following the outage of line 19-20, since there are no DGs and ESSs in the isolated network.

In order to show the dependence of spatial load shedding on the affected lines by the wildfire and the location of DGs and ESSs, an additional case is considered. In *Case IV*, the line 6-26 (and not line 1-2) is considered as the affected line by the fire. The same progression of the wildfire, as in *Case II*, is considered. Fig. 6 corresponds to the distance between the fire and the line 6-26. In this case, the isolated part of the distribution system comprises an ESS at bus 26 and a WT at bus 31.

The expected spatial load shedding for *Cases II* and *IV* are presented in Figs. 14 and 15, respectively. The only difference between the two cases is the affected line. Given that, in *Case II*, the affected line 1-2 isolates the distribution system from the upstream system, the location of DGs and ESSs will not have critical influence on spatial load shedding, unless network lines are congested. In *Case IV* load shedding is recorded at the isolated buses. At the rest of the system, that is connected with the upstream system, the load demand is met by the DGs, the ESS at bus 19 and the power imported from the upstream system. At the isolated part, the ESS at bus 26 and the WT at bus 31 are not able to satisfy the total demand and therefore load has to be shed. If a MT, similar with the one connected at bus 8, was connected at bus 28, no shedding would be recorded in the isolation part. Therefore, it is recognized that the spatial load shedding depends critically on which lines are affected by the wildfire.

VII. Conclusion

This paper has presented a framework for emergency situation, where the outburst of a wildfire threatens the operation of the distribution system. A stochastic mixed integer programming with quadratic constraints is proposed to enhance distribution system resilience through minimizing load shedding. The impact of the wildfire on conductor's temperature and line's functionality are considered. The proposed approach has been illustrated using a modified IEEE 33-bus distribution system. The results show that the resilience of a distribution system against an approaching wildfire is enhanced by considering the progression of the wildfire during distribution system operation. This is essential due to the dependence of the spatial load shedding on the combination of the affected lines by the wildfire and the location of distributed system components, mainly of the DGs and ESSs. Future work will evaluate the contribution of flexible loads in distribution resilience enhancement.

Appendix

Initially, 1000 scenarios have been generated by Monte Carlo simulation. Next, by applying the reduction algorithm, 50, 40, 30, 20 and 10 scenarios have been obtained. The results of the stochastic problem for *Case II* concerning different number of representative scenarios are shown in Table IV. Table IV shows the value of the objective function, the load shedding (most critical variable) and the computation time. Also, the results for the mean values of the stochastic parameters are presented for the case of 1 scenario.

TABLE IV
SIMULATION RESULTS CONCERNING DIFFERENT NUMBER OF REPRESENTATIVE SCENARIOS

Number of scenarios	Objective Function ($\$\times 10^3$)	Load shedding (MWh)	Computation time (s)
1	−64.51	0.653	317.491
10	−63.81	1.23	973.074
20	−63.84	1.21	5281.147
30	−63.79	1.25	10314.548
40	−63.76	1.27	17934.734
50	−63.78	1.26	22487.856

Taking into account that the proposed method is applied when the outburst of a wildfire threatens the distribution system and timely decisions have to be made, 10 scenarios seems to be the best choice. For 10 scenarios, the optimization problem is solved in 973.074 seconds, that is less than the time step of 30 minutes, while the results are similar with the cases where more scenarios are considered.

REFERENCES

[1] A. R. Berkeley, III, and M. Wallace, *A Framework for Establishing Critical Infrastructure Resilience Goals: Final Goals and Recommendations*. Washington, DC, USA: Nat. Infrastruct. Advisory Council, Oct. 2010.

[2] A. Gholami, F. Aminifar, and M. Shahidehpour, "Front lines against the darkness: Enhancing the resilience of the electricity grid through microgrid facilities," *IEEE Electrif. Mag.*, vol. 4, no. 1, pp. 18–24, Mar. 2016.

[3] President's Council of Economic Advisers, "Economic benefits of increasing electric grid resilience to weather outages," Executive Office President, Office Elect. Del. Energy Rel., U.S. Dept. Energy, Washington, DC, USA, Tech. Rep., Aug. 2013.

[4] M. Panteli and P. Mancarella, "The grid: Stronger, bigger, smarter?: Presenting a conceptual framework of power system resilience," *IEEE Power Energy Mag.*, vol. 13, no. 3, pp. 58–66, May/Jun. 2015.

[5] W. Yuan, J. Wang, F. Qiu, C. Chen, C. Kang, and B. Zeng, "Robust optimization-based resilient distribution network planning against natural disasters," *IEEE Trans. Smart Grid*, vol. 7, no. 6, pp. 2817–2826, Nov. 2016.

[6] S. Ma, B. Chen, and Z. Wang, "Resilience enhancement strategy for distribution systems under extreme weather events," *IEEE Trans. Smart Grid*, to be published.

[7] N. R. Romero, L. K. Nozick, I. D. Dobson, N. Xu, and D. A. Jones, "Transmission and generation expansion to mitigate seismic risk," *IEEE Trans. Power Syst.*, vol. 28, no. 4, pp. 3692–3701, Nov. 2013.

[8] A. Gholami, T. Shekari, F. Aminifar, and M. Shahidehpour, "Microgrid scheduling with uncertainty: The quest for resilience," *IEEE Trans. Smart Grid*, vol. 7, no. 6, pp. 2849–2858, Nov. 2016.

[9] A. Khodaei, "Resiliency-oriented microgrid optimal scheduling," *IEEE Trans. Smart Grid*, vol. 5, no. 4, pp. 1584–1591, Jul. 2014.

[10] Z. Wang and J. Wang, "Self-healing resilient distribution systems based on sectionalization into microgrids," *IEEE Trans. Power Syst.*, vol. 30, no. 6, pp. 3139–3149, Nov. 2015.

[11] M. Panteli, D. N. Trakas, P. Mancarella, and N. D. Hatziargyriou, "Boosting the power grid resilience to extreme weather events using defensive islanding," *IEEE Trans. Smart Grid*, vol. 7, no. 6, pp. 2913–2922, Nov. 2016.

[12] M. Panteli and P. Mancarella, "Modeling and evaluating the resilience of critical electrical power infrastructure to extreme weather events," *IEEE Syst. J.*, to be published.

[13] C. Wang, Y. Hou, F. Qiu, S. Lei, and K. Liu, "Resilience enhancement with sequentially proactive operation strategies," *IEEE Trans. Power Syst.*, vol. 32, no. 4, pp. 2847–2857, Jul. 2017.

[14] M. Panteli, P. Mancarella, D. Trakas, E. Kyriakides, and N. Hatziargyriou, "Metrics and quantification of operational and infrastructure resilience in power systems," *IEEE Trans. Power Syst.*, to be published.

[15] A. Bagchi, A. Sprintson, and C. Singh, "Modeling the impact of fire spread on the electrical distribution network of a virtual city," in *Proc. 41st North Amer. Power Symp.*, Starkville, MS, USA, 2009, pp. 1–6.

[16] M. Choobineh, B. Ansari, and S. Mohagheghi, "Vulnerability assessment of the power grid against progressing wildfires," *Fire Safety J.*, vol. 73, pp. 20–28, 2015.

[17] S. Mohagheghi and S. Rebennack, "Optimal resilient power grid operation during the course of a progressing wildfire," *Int. J. Elect. Power Energy Syst.*, vol. 73, pp. 843–852, 2015.

[18] B. Ansari and S. Mohagheghi, "Optimal energy dispatch of the power distribution network during the course of a progressing wildfire," *Int. Trans. Elect. Energy Syst.*, vol. 25, pp. 3422–3438, 2015.

[19] *IEEE Standard for Calculating the Current-Temperature Relationship of Bare Overhead Conductors*, IEEE Std 738-2012 (Revision of IEEE Std 738-2006 - Incorporates IEEE Std 738-2012 Cor 1-2013), Dec. 23, 2013, pp. 1–72.

[20] European Distribution System Operators for Smart Grids, "Coordination of transmission and distribution system operators: A key step for the Energy Union," May 2015.

[21] N. Hatziargyriou *et al.*, "Contribution to bulk system control and stability by distributed energy resources connected at distribution network," IEEE Power Energy Soc., Piscataway, NJ, USA, Tech. Rep. TR-22, 2017.

[22] W. Bartels *et al.*, "Generating plants connected to the medium-voltage network," *Tech. Guideline of BDEW*, 2008. [Online]. Available: https://www.bdew.de/internet.nsf/id/A2A0475F2FAE8F44C12578300047C92F/$file/BDEW_RL_EA-am-MS-Netz_engl.pdf

[23] The distribution code of licensed distribution network operators of Great Britain, 2017. [Online]. Available: http://www.dcode.org.uk/

[24] G. Sideratos and N. D. Hatziargyriou, "Probabilistic wind power forecasting using radial basis function neural networks," *IEEE Trans. Power Syst.*, vol. 27, no. 4, pp. 1788–1796, Nov. 2012.

[25] Z. Liu, F. Wen, and G. Ledwich, "Optimal siting and sizing of distributed generators in distribution systems considering uncertainties," *IEEE Trans. Power Del.*, vol. 26, no. 4, pp. 2541–2551, Oct. 2011.

[26] S. A. Arefifar, Y. A. R. I. Mohamed, and T. H. M. El-Fouly, "Supply-adequacy-based optimal construction of microgrids in smart distribution systems," *IEEE Trans. Smart Grid*, vol. 3, no. 3, pp. 1491–1502, Sep. 2012.

[27] W. Li, *Risk Assessment of Power Systems: Models, Methods, and Applications*. New York, NY, USA: Wiley, 2005

[28] H. Heitsch and W. Römisch, "Scenario reduction algorithms in stochastic programming," *Comput. Optim. Appl.*, vol. 24, nos. 2/3, pp. 187–206, Feb. 2003.

[29] J. L. Rossi, A. Simeoni, B. Moretti, and V. Leroy-Cancellieri, "An analytical model based on radiative heating for the determination of safety distances for wildland fires," *Fire Safety J.*, vol. 46, pp. 520–527, 2011.

[30] P. A. Trodden, W. A. Bukhsh, A. Grothey, and K. I. M. McKinnon, "Optimization-based islanding of power networks using piecewise linear AC power flow," *IEEE Trans. Power Syst.*, vol. 29, no. 3, pp. 1212–1220, May 2014.

[31] C. Coffrin and P. V. Hentenryck, "A linear-programming approximation of ac power flows," *INFORMS J. Comput.*, vol. 26, no. 4, pp. 718–734, May 2014.

[32] M. Nick, O. Alizadeh-Mousavi, R. Cherkaoui, and M. Paolone, "Security constrained unit commitment with dynamic thermal line rating," *IEEE Trans. Power Syst.*, vol. 31, no. 3, pp. 2014–2025, May 2016.

[33] C. Wang and H. Z. Cheng, "Optimization of network configuration in large distribution systems using plant growth simulation algorithm," *IEEE Trans. Power Syst.*, vol. 23, no. 1, pp. 119–126, Feb. 2008.

[34] E. E. Sfikas, Y. A. Katsigiannis, and P. S. Georgilakis, "Simultaneous capacity optimization of distributed generation and storage in medium voltage microgrids," *Int. J. Elect. Power Energy Syst.*, vol. 67, pp. 101–113, May 2015.

[35] D. I. Papaioannou, C. N. Papadimitriou, A. L. Dimeas, E. I. Zountouridou, G. C. Kiokes, and N. D. Hatziargyriou, "Optimization & sensitivity analysis of microgrids using HOMER software—A case study," in *Proc. MedPower 2014*, Athens, Greece, 2014, pp. 1–7.

[36] PVWatts Calculator. 2016. [Online]. Available: http://pvwatts.nrel.gov

[37] D. M. Greenwood, G. L. Ingram, and P. C. Taylor, "Applying wind simulations for planning and operation of real-time thermal ratings," *IEEE Trans. Smart Grid*, vol. 8, no. 2, pp. 537–547, Mar. 2017.

[38] H. Farzin, M. Fotuhi-Firuzabad, and M. Moeini-Aghtaie, "Stochastic energy management of microgrids during unscheduled islanding period," *IEEE Trans. Ind. Informat.*, vol. 13, no. 3, pp. 1079–1087, Jun. 2017.

Dimitris N. Trakas (S'16) received the Diploma in electrical and computers engineering and the Master of Sciences degree in energy production and management from the National Technical University of Athens (NTUA), Athens, Greece, in 2009 and 2011. He is currently working toward the Ph.D. degree with the Electric Power Division at NTUA. His research interests include decentralized control of power systems, resilience assessment, and enhancement of power systems.

Nikos D. Hatziargyriou (F'09) is the Chairman and CEO of the Hellenic Distribution Network Operator. Since 1984, he has been with the Power Division of the Electrical and Computer Engineering Department, National Technical University of Athens, Athens, Greece, where he has been a full Professor in power systems since 1995. From February 2007 to September 2012, he was the Deputy CEO of the Public Power Corporation of Greece, responsible for Transmission and Distribution Networks, island DNO, and the Center of Testing, Research and Prototyping. He has authored the book entitled *Microgrids: Architectures and Control* and more than 200 journal publications and 500 conference proceedings papers.

Prof. Hatziargyriou is the past Chair of the Power System Dynamic Performance Committee, an Honorary Member of CIGRE, and the past Chair of CIGRE SC C6 "Distribution Systems and Distributed Generation." He is the co-chair of the EU Technology and Innovation Platform on Smart Networks for Energy Transition. He is a member of the Energy Committee of the Athens Academy of Science. He has participated in more than 60 R&D Projects funded by the EC and the industry and has coordinated, among others, the EU "CARE," "MORE CARE," "MERGE," "Microgrids," and "More Microgrids" projects. He is the Editor-in-Chief of the IEEE TRANSACTIONS ON POWER SYSTEMS and a member of the Editorial Board of the IEEE TRANSACTIONS ON SUSTAINABLE DEVELOPMENT and the IEEE POWER AND ENERGY MAGAZINE. He is included in the 2016 Thomson Reuters' list of the top 1% most cited researchers.